Pol. J. Environ. Stud. Vol. XX, No. X (XXXX), 1-13
DOI: *10.15244/pjoes/213560* ONLINE PUBLICATION DATE: 2026-01-08

Original Research

An Innovative Geopolymer Composite Insulation Material Based on Phytoremediation Biowaste: Solidification/Stabilization of Potentially Toxic Metals

Juan Du[1], Jinfeng Shi[1], Lei Zhang[2]*, Xianghong Ren[1], Jing Dong[1], Shuai Yang[1], Jiapeng Liu[1]

[1]Rocket Force University of Engineering, Xi'an, Shaanxi 710025, China
[2]Xi'an Thermal Power Research Institute Co., Ltd., Xi'an, Shaanxi 710054, China

Received: 06 July 2025
Accepted: 23 October 2025

Abstract

Phytoremediation biowaste without proper disposal might release potentially toxic metals (PTMs) back into the environment and pose a serious threat to environmental safety and human health. A composite geopolymer based on phytoremediation biowastes (PBWs) was used to effectively solidify/stabilize toxic heavy metals and served as an insulation material in the present study. For the solidification/stabilization of PTMs, the optimum proportion of biowastes in the geopolymer insulation material was 3%, at which the compressive strength of the geopolymer reached a maximum of 32.6 MPa and the thermal conductivity of the geopolymer was 0.11 W/(m·K), meeting the requirements of insulation materials. The leaching results indicated that the solidification efficiency of PTMs in the geopolymer materials was over 98%. The leaching concentration of all samples was within the standard limits and decreased with the extension of curing time. The XRD and FT-IR spectra of the biowaste-geopolymer confirmed the effective solidification/stabilization of PTMs in the geopolymer composite, where Zn was immobilized as carbonate and silicate. The geopolymer technique can stabilize the PTMs and prepare insulation materials simultaneously. Hence, this research provided a helpful insight and theoretical support for the post-treatment and the reutilization of plant waste accumulated with heavy metals.

Keywords: phytoremediation biowastes, potentially toxic metals, geopolymer, solidification/stabilization, insulation

*e-mail: 89314553@qq.com
Tel.: 86 18066705283
ORCID iD: 0009-0008-5709-5529

Introduction

Phytoremediation is an environmentally friendly and effective technique for remediating soil that is contaminated by potentially toxic metals (PTMs) [1-4]. Nevertheless, the potentially toxic metals (PTMs) accumulated in the harvested phytoremediation plant might be a barrier to the wide application of soil phytoremediation in cases where the biowaste is not properly disposed of. The biowaste not only occupies massive land, but also releases toxic metals back into the environment and poses a serious threat to environmental safety and human health [2, 4-6].

Various post-processing approaches for phytoremediation biowaste have been studied, including composting, liquid phase extraction, hydrothermal liquefaction, combustion, pyrolysis, etc. During the composting process, the volume of biowaste residues can be reduced, the contained toxic metals can be transformed into more stable chemical forms, and the biowaste can be converted into organic fertilizers [7]. However, composting is a time-consuming and costly process; the total amount of toxic metals in the compost products has not changed, and its subsequent treatment still needs to be further studied. The liquid phase extraction method is to extract PTMs from the plant by dissolution or chelation using a suitable extractant, such as strong acids [8], chelating agents, organic solvents, and inorganic salt solutions [9]. However, generally, a single extractant can only extract certain heavy metals, which is not suitable for the actual post-treatment of phytoremediation plants. Ascribing to the limits of process equipment and reaction conditions, the liquid phase extraction technique has not been widely applied. Hydrothermal liquefaction is a type of supercritical water technology. Due to the high temperature and high pressure, the molecular bonds of hydrocarbons in the biomass are broken, and the organic components are transformed into small molecular substances, resulting in water-soluble products, which can form oils after condensation, and then form charcoal after further condensation [10]. Hydrothermal liquefaction can not only reduce the biomass volume and transfer PTMs into the liquid phase but also produce bio-oil. Additionally, Jiang et al. [11] presented a practicable route for the disposal of As-enriched biomass via one-pot hydrothermal treatment with the assistance of $CaO/Ca(ClO)_2$, which can transfer As from the aqueous phase to the solid phase (hydrochar), as well as promote the transformation of As(III) to As(V). Nonetheless, the equipment requirements of this technology are considerably strict, and the reaction sediment can easily cause equipment breakdown. Thus, it still needs further study, although the reaction rate of this technology is fast and offers good economic benefits. Combustion can significantly reduce the volume of biowaste at high temperatures and recover the heat simultaneously. Nevertheless, PTMs in the biowaste can easily escape with fly ash at high temperatures. Sui et al. [12] found that PTMs in the bottom ash decreased with the increase of temperature, while increasing in fly ash at the same time, and Ca, with its high content in plants, had a positive effect on the solidification of heavy metals. The major heavy metals Zn, Pb, and Cd were all above the emission limits of the EU standard, and the release rate of heavy metals increased to 70% for cadmium as the combustion temperature increased. Therefore, high temperatures limit the application of combustion technology. Pyrolysis has been employed for biowaste disposal, which can minimize the bulk volume of biowaste and generate bioenergy (including biochar, biomass oil, and gas). Many studies have shown that PTMs tend to accumulate in the biochar during pyrolysis [10, 13-15]. Although biochar has been widely used in agricultural fields to improve soil fertility, enhance soil water retention, and remediate soil contaminated by PTMs [16], the application of biochar containing PTMs is still a challenge. Li et al. [17] attempted to obtain heavy-metal-free and phosphorus-rich biochar from phytoremediation residue (PR) by pyrolysis with chlorinating agent addition. Although the concentration of Zn in biochar was reduced to one-tenth of that in PR by intensified chlorination, the metal chloride pollution in the flue gas has emerged as another challenging issue that needs to be addressed. Solidification/stabilization (S/S) is recognized as a highly effective, stable, gentle, and environmentally friendly approach for the disposal of solid waste containing PTMs, which can fix the hazardous waste in the products; thus, the solubility of PTMs in the products can be greatly reduced for safe application [18-21]. In the 1990s, the French scholar Davidovits [22] proposed a new type of material – geopolymer, which is based on active aluminosilicate and alkali activator (NaOH or $NaHCO_3$, etc.) as the main raw materials, mixed in appropriate proportions. Under appropriate reaction and curing conditions, "zeolite-like" structural materials (geopolymer) with considerable strength can be obtained. Compared with ordinary Portland cement, geopolymers have the advantages of low carbon emission, strong mechanical properties, oxidation resistance, fire resistance, corrosion resistance, high thermal stability and impermeability, and strong solidification ability of metal ions [23-28]. At present, the aluminosilicate raw materials that can be used for the preparation of geopolymers include metakaolin, fly ash, incineration fly ash, blast furnace slag, etc. These raw materials are widely available and easy to obtain. In recent years, geopolymers have been extensively studied and applied in the field of solidification/stabilization of heavy metals, such as metal smelting slag, tailing slag, municipal solid waste incineration fly ash, drinking water treatment residuals, coal gasification fly ash or coarse slag, and others [23, 29-35]. Researchers generally focused on the industrial solid waste containing heavy metals; there are few reports on the application of geopolymers for heavy metal solidification/stabilization in the post-treatment

of phytoremediation biowaste. Therefore, it is proposed that heavy metal-enriched plants be solidified using geopolymers, given their significant potential for environmental protection.

The objectives of our investigation were to (1) analyze the effect of biowaste on the compressive strength of geopolymer composites; (2) display the insulation performance of geopolymer composites with the addition of biowaste; (3) evaluate the PTMs' solidification/stabilization behavior in the geopolymer composites; (4) elucidate the solidification/stabilization mechanism of biowaste by geopolymer. This research tries to explore an innovative approach for the post-treatment of phytoremediation biowaste, which can not only solidify the PTMs but also enable the development of a credible geopolymer composite insulation material. The effective and environmentally friendly disposal of phytoremediation biowaste by geopolymer is expected to promote the further development of phytoremediation techniques.

Materials and Methods

Materials

The phytoremediation biowaste, metakaolin (MK), sodium silicate (SS), and NaOH were used as raw materials in geopolymer preparation. The phytoremediation biowaste – *Silphium perfoliatum* L. samples (abbreviated as SP) – was obtained from a heavy-metal-polluted area in Fengxian County (33°34′57″–34°18′21″E, 106°24′54″–107°7′30″N), Shaanxi Province, China. The soil here was seriously polluted by Pb and Zn due to mining and smelting activities in the local area [3]. The harvested biowaste was washed with distilled water, dried in an oven, and ground into powder with a particle size of <0.15 mm. The prepared samples were kept in airtight bags for further utilization [36]. High-purity metakaolin was used as a precursor, and its chemical composition was determined by an X-ray fluorescence spectrometer (XRF), as illustrated in Table S1 (Supplementary Information). The sodium silicate solution (with a silica-to-sodium oxide molar ratio of 3.3) and NaOH (AR, 97%, Aladdin, China) were applied as alkaline activators. Deionized water was used for solution preparation in this study.

Preparation of Geopolymer

Geopolymer batches of various compositions were prepared according to the proportions shown in Table 1. Each geopolymer batch was prepared by mixing biowaste and metakaolin, with a total weight of 150 g, and the proportion of biowaste was 0 wt.%, 1 wt.%, 3 wt.%, 5 wt.%, 7 wt.% and 9 wt.%, respectively. Based on the pre-experimental results, the molar ratios of SiO_2/Al_2O_3 and Na_2O/Al_2O_3 were set to 3.05 and 0.8, respectively. The solid-to-liquid (S/L) ratio was maintained at 1.84 to obtain a geopolymer paste with good workability.

For sample preparation, the biowaste was dried, ground, and thoroughly mixed with metakaolin. The alkali activator solution was prepared by dissolving NaOH reagent in sodium silicate (modulus = 3.3) and distilled water, and aged for 12 h to promote the polymerization of sodium silicate [37]. Then, the resultant solution was blended with the solid mixture completely using an automatic blender to obtain a uniform paste. The fresh pastes were transferred into plastic cube molds (40×40×40 mm³), vibrated for 10 minutes to remove air bubbles, and sealed with plastic film and cured for 24 h at room temperature [38, 39]. The shaped cubic geopolymer specimens were demolded, marked, and then cured in a maintenance box at 20°C and 90% RH for 7, 14, and 28 days, respectively. All geopolymer batches were prepared in triplicate. The specimens with biowaste addition of 0 wt.%, 1 wt.%, 3 wt.%, 5 wt.%, 7 wt.% and 9 wt.% were recorded as BK0, BK1, BK3, BK5, BK7 and BK9, respectively.

Characterization of Geopolymer Composites

Compressive Strength Test

The mechanical strength of the cubic geopolymer specimens was measured by the compressive strength

Table 1. Proportions of raw materials for geopolymer preparation.

Sample code	Metakaolin (g)	Biowaste (wt.%)	Biowaste (g)	Sodium silicate (g)	NaOH (g)	Water (g)
BK0	150	0	0	204.1	23.94	0
BK1	148.5	1	1.5	202.0	23.70	0.813
BK3	145.5	3	4.5	197.9	23.22	2.443
BK5	142.5	5	7.5	193.9	22.74	4.072
BK7	139.5	7	10.5	189.8	22.26	5.702
BK9	136.5	9	13.5	185.7	21.78	7.331

Note: BK0, BK1, BK3, BK5, BK7, and BK9 represent the bio-geopolymer insulation materials with biomass additions of 0 wt.%, 1 wt.%, 3 wt.%, 5 wt.%, 7 wt.%, and 9 wt.%, respectively.

testing method. After 28-day curing, the compressive strength of the cubic geopolymer specimens was tested by an Electronic Universal Testing Machine (WDW-300, Jinan, China) with a load displacement rate of 10 mm/min. Each cubic geopolymer specimen was tested in triplicate, and the average value was obtained for further analysis.

Thermal Conductivity Measurement

The thermal insulation performance of the geopolymer specimens was assessed based on thermal conductivity measurements. Thermal conductivity (λ) was determined by a thermal conductivity test device (FD-TC-B, Tianxin, China) at an environmental temperature of 20ºC, which is a non-destructive test based on the hot plate method, referring to Thermal Insulation-Determination of Steady-State Thermal Resistance and Related Properties [40]. The geopolymer specimens for thermal conductivity measurement were disc-shaped with dimensions of *Φ*10 cm×1 cm. All the specimens were dried and polished before the test. The measurement was done by placing the specimen between the heating plate and the cooling plate. Tests were performed in triplicate for all specimens, and the results were averaged.

Leaching Test

The solidification/stabilization (S/S) efficiency of PTMs (Pb and Zn) in geopolymer specimens was characterized by the leaching test according to the standard toxicity characteristic leaching procedure (TCLP) [41] and the standard synthetic precipitation leaching procedure (SPLP) [42]. TCLP is generally used to simulate the leaching conditions in landfills, and SPLP is suggested to simulate the natural acid rain environment [13]. The fragments of each geopolymer specimen were collected from the compressive strength test and crushed into granules with a size of less than 9.5 mm. The resultant leachates were filtered and stored for PTMs (Pb and Zn) determination by atomic absorption spectrometer (Z-2000, Hitachi, Japan) according to GB5085.3-2007 [43]. Reagent blanks were prepared for each batch of samples. S/S efficiency (f) was determined as follows:

$$f = (C_0 - C_f)/C_0 \times 100\%$$

where C_0 represents the initial PTMs' total concentration before solidification, and C_f represents the leaching concentration after solidification [1, 39, 44, 45]. The total content of PTMs in the solid materials was determined by the wet digestion method [46].

Microstructure

In order to investigate the micro-characteristics of geopolymer specimens, the crushed specimens were collected from the strength test and further milled into fine powders, and then dried in an oven at 80°C for 48 h. X-ray diffraction (XRD) analysis was performed by an X-ray diffractometer (XRD, Rigaku Ultima IV, Japan) with a Cu-Kα radiation source in the 2ɵ range of 10º to 80º (scanning rate, $5^{o} \cdot min^{-1}$). The chemical bonds of hydration products in the geopolymer specimens were analyzed by Fourier-transform infrared spectroscopy (FTIR, Bruker, Germany) over the infrared range of 4000-400 cm^{-1}.

Quality Control and Statistical Analysis

All analyses were conducted in triplicate, and blank samples were used for correction of test results. Statistical analysis was performed using SPSS 23.0 software. All figures were prepared using OriginPro software (version 2024).

Results and Discussion

Effect of Biowaste on Compressive Strength

Compressive strength can be used to characterize the mechanical properties and structural stability of the geopolymer specimens based on the phytoremediation biowaste [39]. Compressive strength development of the geopolymer specimens cured for 28 days with various biowaste content (0 wt.%, 1 wt.%, 3 wt.%, 5 wt.%, 7 wt.%, and 9 wt.%) was shown in Fig. 1. It can be seen that the compressive strength of the bio-geopolymer composites increased first and then decreased with increasing biomass addition. The compressive strength reached the maximum of 32.6 MPa when 3 wt.% of biomass was added. After that, the compressive strength of the composite decreased significantly with the increase in biomass addition. The analysis results of significant differences in compressive strength indicated that the compressive strength of BK3 (biomass addition of 3 wt.%) was significantly higher than other specimens; the compressive strength differences among BK0, BK1, and BK5 were not particularly significant. The compressive strength of BK7 and BK9 was significantly lower than that of the composite with less biomass addition. Biomass is characterized by fiber structure and toughness. A certain amount of addition of biomass can play the role of a bridge in the interior of the geopolymer composite, preventing crack propagation and improving the mechanical properties of the geopolymer composite [47, 48]. However, as the amount of biomass increased further, the content of metakaolin, which is the active component in the geopolymer, decreased correspondingly in the case of a constant proportion of geopolymer raw materials. Thus, less geopolymer gel was obtained, and the density of the geopolymer composite decreased, which affected the mechanical properties of the composite and reduced its compressive strength [49]. Another possibility

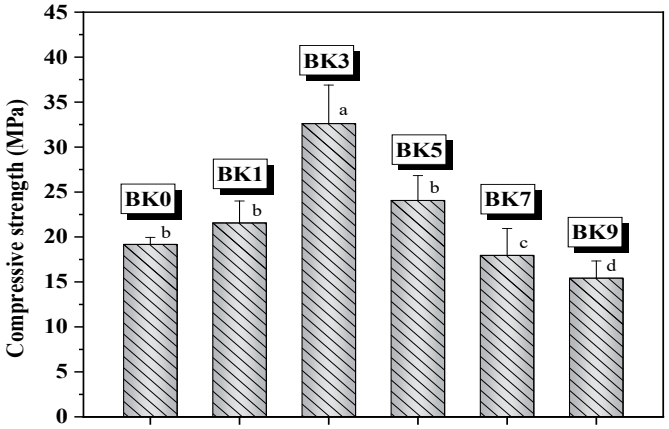

Fig. 1. Compressive strength of bio-geopolymer insulation materials with various biomass contents.
Note: BK0, BK1, BK3, BK5, BK7, and BK9 represent the bio-geopolymer insulation materials (28-day curing) with biomass additions of 0 wt.%, 1 wt.%, 3 wt.%, 5 wt.%, 7 wt.% and 9 wt.%, respectively.

is that greater introduction of PTMs generates more PTM hydroxyl complex ions, which might interfere with the condensation reaction of aluminum or silicon oxide tetrahedra, and thereby reduce the formation of the geopolymer gel structure [47, 50].

Wang [50] studied the effect of rice husk on the compressive strength of geopolymer insulation material and found that the compressive strength of the material increased significantly as the amount of rice husk increased from 0 to 10 wt.%, and then as the proportion of biomass increased continuously, the compressive strength of the material continued to decrease. Ye et al. [48] reported that the compressive strength of the fiber-geopolymer materials was higher with 5 wt.% of lignin, cellulose, or hemicellulose addition than that with proportions of 10 wt.% or 20 wt.%. Zheng et al. [47] also demonstrated that the compressive strength of the geopolymer with 2% bamboo cellulose increased by 85.1% after 30 days. Therefore, this observation is validated in the present study, showing that a certain amount of biowaste (3 wt.%) addition can improve the mechanical properties of geopolymer specimens based on phytoremediation biowaste. In addition, the compressive strength of the biomass-geopolymer composite materials in this study meets the requirements (not less than 0.2~0.4 MPa) in the standard of Dry-mixed Thermal Insulating Composition for Buildings [51].

Effect of Biowaste on Insulation Performance

Thermal conductivity is used to evaluate the insulation performance of a geopolymer composite based on the biowaste. Fig. 2 shows the effect of biomass addition on the thermal conductivity of geopolymer composites cured for 28 days. As can be seen, the thermal conductivity of the biomass-geopolymer composite decreased gradually with increasing biomass addition; that is, the thermal insulation performance of

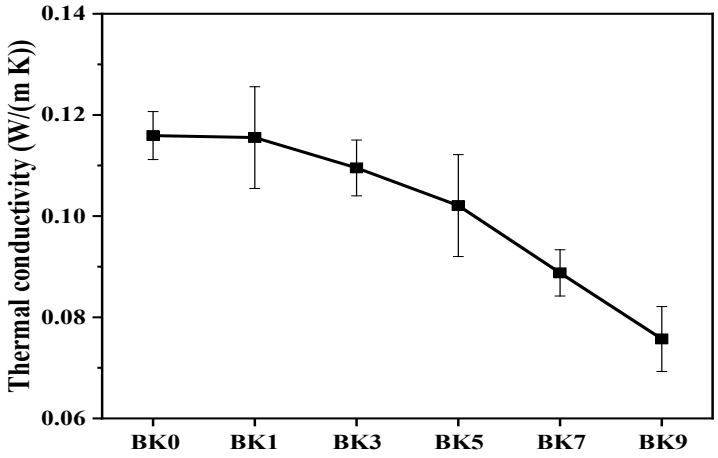

Fig. 2. Thermal conductivity of biomass-geopolymer insulation materials with different biomass contents.
Note: BK0, BK1, BK3, BK5, BK7, and BK9 represent the biomass-geopolymer insulation materials (28-day curing) with biomass additions of 0 wt.%, 1 wt.%, 3 wt.%, 5 wt.%, 7 wt.%, and 9 wt.%, respectively.

the biomass-geopolymer composite was continuously improved. The thermal conductivity of the material is mainly associated with pore size and pore distribution in the material. Generally, biomass is porous due to its fibrous structure and has a lower thermal conductivity than the geopolymer [24, 49]. Moreover, when the biomass addition was 9 wt.% in this study, the thermal conductivity of the composite decreased to 0.076 W/(m·K), meeting the required value of 0.085 W/(m·K) (ambient temperature 25ºC) in the standard of Dry-mixed Thermal Insulating Composition for Buildings [51]. The experimental study of biomass geopolymer-based insulation materials (including wheat straw, rice husk, and sawdust) by Wang et al. [52] also reported that the thermal conductivities of wheat straw/geopolymer, rice husk/geopolymer, and sawdust/geopolymer were 0.104 W/(m·K), 0.107 W/(m·K), and 0.089 W/(m·K), respectively, with about 10 wt.% of biomass addition. The thermal conductivity of the geopolymer composites obtained in the present study is comparable to that of the commercially available thermal insulation materials such as thermal insulation mortar for buildings (~0.07 W/(m·K)), expanded perlite thermal insulation material (~0.087 W/(m·K)), aluminum silicate refractory fiber (0.116 W/(m·K)), and ceramic thermal insulation material (~0.08 W/(m·K)). Consequently, the biomass-geopolymer composite prepared in this study may be a promising insulation material for use in the construction field.

Meanwhile, the compressive strength of the biomass-geopolymer composites was 32.6 MPa, 23.8 MPa, 17.9 MPa, and 15.5 MPa when the biomass addition was 3 wt.%, 5 wt.%, 7 wt.%, and 9 wt.%, respectively. The thermal conductivity of the composites was 0.11 W/(m·K), 0.102 W/(m·K), 0.088 W/(m·K), 0.076 W/(m·K) when the addition of biomass was 3 wt.%, 5 wt.%, 7 wt.%, and 9 wt.%, respectively. As BK3 (3 wt.% biomass addition) had the maximum compressive strength and comparable thermal conductivity to commercially available thermal insulation materials, the amount of biomass added was suggested to be 3 wt.% in the biomass-geopolymer composite and thus has potential as an insulation material for buildings.

Table 2. Leaching concentration and S/S efficiency of Zn in the geopolymer specimens.

Specimens	TCLP		SPLP	
	Leaching concentration (mg L^{-1})	S/S efficiency (%)	Leaching concentration (mg L^{-1})	S/S efficiency (%)
BK0-7d	ND	-	ND	-
BK1-7d	0.0420±0.0014	98.05	0.0205±0.0007	99.05
BK3-7d	0.1275±0.0021	98.03	0.0575±0.0014	99.11
BK5-7d	0.2105±0.0021	98.05	0.0985±0.0007	99.09
BK7-7d	0.2770±0.0099	98.17	0.1395±0.0021	99.08
BK9-7d	0.3830±0.0028	98.02	0.1735±0.0021	99.11
BK0-14d	ND	-	ND	-
BK1-14d	0.0380±0.0028	98.24	0.0175±0.0007	99.19
BK3-14d	0.1240±0.0042	98.08	0.0565±0.0049	99.13
BK5-14d	0.1995±0.0050	98.15	0.0955±0.0035	99.11
BK7-14d	0.2700±0.0085	98.21	0.1380±0.0057	99.09
BK9-14d	0.3690±0.0099	98.10	0.1650±0.0028	99.15
BK0-28d	ND	-	ND	-
BK1-28d	0.0340±0.0028	98.42	0.0140±0.0014	99.35
BK3-28d	0.1105±0.0064	98.29	0.0440±0.0042	99.32
BK5-28d	0.1820±0.0042	98.31	0.0785±0.0035	99.27
BK7-28d	0.2415±0.0050	98.40	0.1305±0.0021	99.14
BK9-28d	0.2885±0.0078	98.51	0.1615±0.0078	99.17
Limited values by US EPA	25		25	
GB 5085.3-2007	-		100	

Note: ND, not detected. BK0, BK1, BK3, BK5, BK7, and BK9 represent the biomass-geopolymer insulation materials with biomass additions of 0 wt.%, 1 wt.%, 3 wt.%, 5 wt.%, 7 wt.%, and 9 wt.%, respectively.

Evaluation of PTMs Solidification/Stabilization

The batch leaching test (TCLP or SPLP) could effectively evaluate the leaching performance of PTMs simulating their instant leaching behavior in landfill and acid rain environments. Pb had not been detected in each extract, as the content of Pb was not too high in the raw material, and it had been solidified in the geopolymer material completely. Table 2 and Fig. 3 illustrate the leaching concentration and S/S efficiency of Zn in the biomass-geopolymer composite with various biomass contents, curing for 7 d, 14 d, and 28 d, respectively. It can be seen from Table 2 that the leaching concentration of Zn in the geopolymers increased gradually with the increment of biomass proportion when experiencing the same curing time. The leaching concentration of Zn ranged from 0 to 0.3830 mg·L^{-1} in the TCLP test, and 0 to 0.1735 mg·L^{-1} in the SPLP test, respectively. Although different leaching conditions with varying pH values and ionic strength were performed, Zn leachabilities of all biomass-geopolymer composites were below 25 mg·L^{-1} as specified in Table 2, indicating that all specimens in the present study could comply with the limited values by the US EPA and the Chinese leaching standard for hazardous wastes (GB 5085.3-2007) [43, 44]. Referring to a certain specimen, extending the curing time could significantly reduce the Zn leachability as depicted in Fig. 3. For instance, the leaching concentration of Zn in the BK9 specimen reduced from 0.3830 mg·L^{-1} to 0.2885 mg·L^{-1} for the TCLP test and from 0.1735 mg·L^{-1} to 0.1615 mg·L^{-1} for the SPLP when prolonging the curing time from 7 days to 28 days. Previous studies had also demonstrated that the increased curing time could play a crucial role in PTMs' leaching performance, probably reducing water permeability and porosity of the geopolymer composite, then resulting in PTMs' solidification/stabilization reinforcement [18, 35, 38, 44, 53]. Ji and Pei [32] investigated the blast-furnace slag geopolymers and demonstrated that the leaching concentrations of Cd, Pb, and Zn in the geopolymers cured for 28 days in TCLP, H_2O, NaCl, or other leaching solutions were all lower than those of the materials cured for 7 days. An et al. [54] also found that when the curing

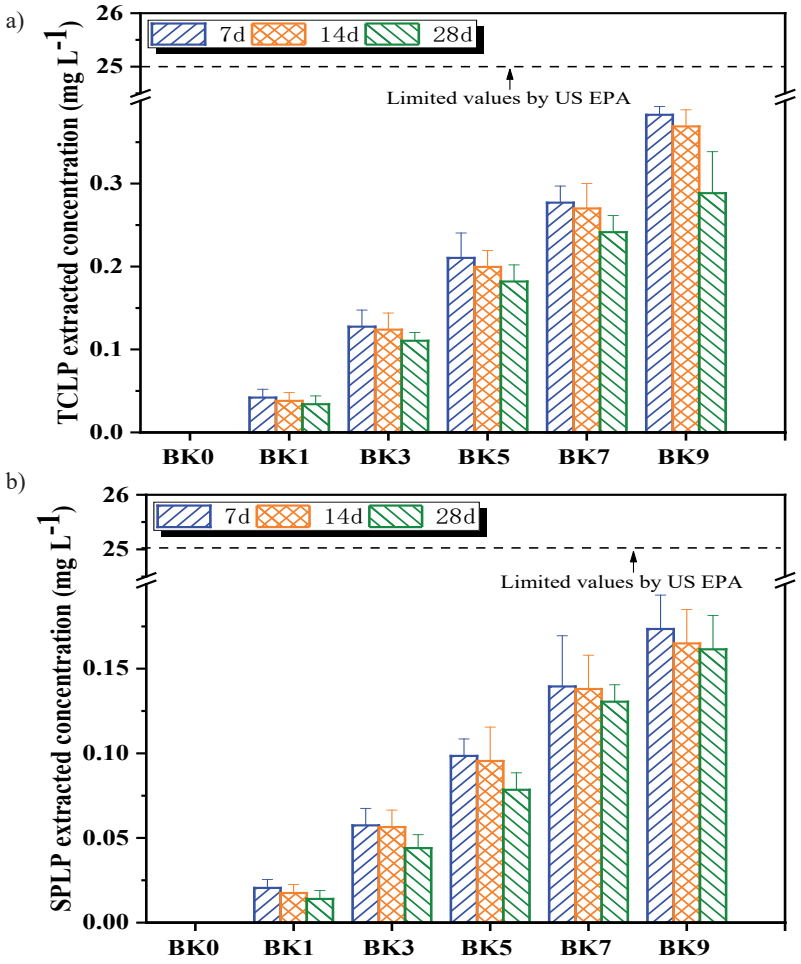

Fig. 3. Leaching concentration of Zn from biomass-geopolymer at different curing times. a) TCLP extracted concentration; b) SPLP extracted concentration.
Note: BK0, BK1, BK3, BK5, BK7, and BK9 represent the biomass-geopolymer insulation materials with biomass additions of 0 wt.%, 1 wt.%, 3 wt.%, 5 wt.%, 7 wt.%, and 9 wt.%, respectively.

period of the geopolymer based on municipal solid waste incineration fly ash increased from 28 days to 60 days, the solidification effect of Zn, Pb, Cd, Cu, and Ni was significantly improved. Geopolymers are formed by silica-oxygen tetrahedrons (SiO_4^-) and alumina-oxygen tetrahedrons (AlO_4^-), connecting through shared oxygen atoms to create a three-dimensional network structure. During the early curing stage (e.g., 7 days), the network structure was not yet completely developed, with numerous defects and unreacted active sites present. As the curing time extended to 14 and 28 days, the silico-aluminous raw materials underwent further dissolution, and the polycondensation reaction continued, leading to a gradual densification of the network structure and a reduction in defects. This structural refinement enhanced the ability to physically entrap heavy metal ions within cavities or adsorb them onto the network surface, thereby significantly reducing leaching risks and elevating the solidification rate. Meanwhile, chemical bonding was further strengthened, contributing to continuous solidification enhancement.

In order to evaluate the S/S efficiency of Zn, the total content of Zn in the geopolymer specimens was determined [46]. The total content of Zn in BK1, BK3, BK5, BK7 and BK9 was 90.80 mg·kg^{-1}, 272.4 mg·kg^{-1}, 453.9 mg·kg^{-1}, 635.6 mg·kg^{-1} and 817.2 mg·kg^{-1}, respectively, and was not detected in BK0. The S/S efficiency of Zn in the geopolymers was presented in Table 2. As for the geopolymer specimens with different biomass additions at the same curing time, almost negligible differences were observed in the S/S efficiency of Zn either in the TCLP test or in the SPLP test. Moreover, a little increase in the S/S efficiency of Zn was observed when the curing time was extended, corresponding to the leaching performance of Zn. In addition, the presented S/S efficiency of Zn in the SPLP test was a little higher than that in the TCLP test, mostly ascribing to the lower pH values of the leaching solution in the TCLP test, which is more favorable for PTMs dissolving. Regardless of the leaching environment, the S/S efficiency of Zn in the geopolymer specimens was up to 98%, confirming the superior immobilization performance of PTMs in the geopolymer composite based on phytoremediation biowaste. The effective solidification of PTMs by the geopolymer is mainly associated with the microstructure and composition of the geopolymer matrix. The existence of biomass could increase the pore size range compared with the specimens without biomass. The increased pore size range might provide more available surfaces for PTMs adsorption [53], and the special three-dimensional network structure in the geopolymer is able to effectively encapsulate the PTMs [20, 55]. Besides, it has been demonstrated that there were electronegative $[AlO(OH)_4]^-$ ions in the geopolymer matrix, thereby some cations (such as Na^+, K^+, Ca^{2+}, Pb^{2+}, Zn^{2+}) were needed to combine with $[AlO(OH)_4]^-$ for charge balancing [18, 34, 55], which provided another probable path for adsorption of PTMs.

Solidification/Stabilization Mechanism of Biowaste by Geopolymer

X-ray Diffraction Analysis

In order to reveal the effect of biomass addition and curing time on the crystal structure of geopolymer specimens, the X-ray diffraction patterns of BK0-28d, BK3-28d, BK9-28d, and BK9-7d specimens were shown

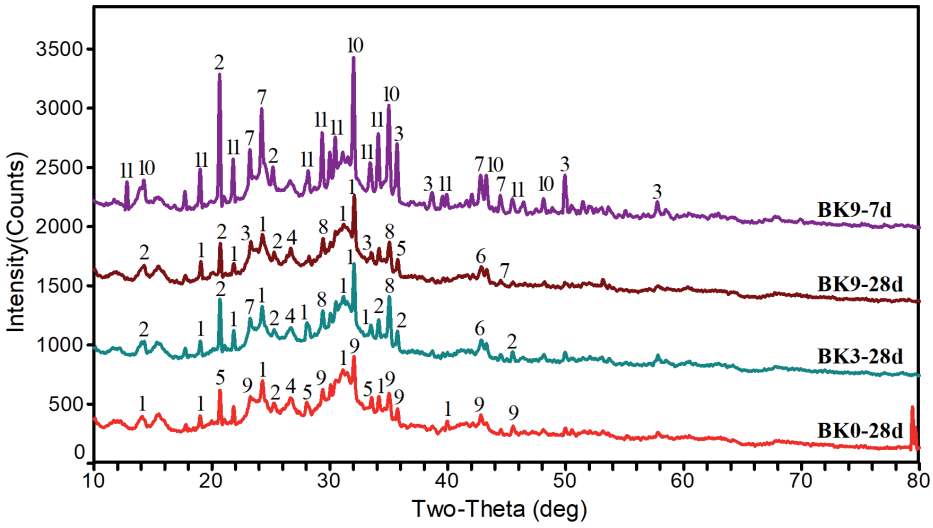

Fig. 4. XRD spectra of biomass-geopolymer.
Note: BK0-28d, BK3-28d, and BK9-28d represent the biomass-geopolymer curing for 28 days with biomass additions of 0 wt.%, 3 wt.%, and 9 wt.%, respectively; BK9-7d represents the biomass-geopolymer curing for 7 days with biomass addition of 9 wt.%. 1-$Ca_2Al_3(Si_3O_{12})(OH)$; 2-$NaAlSi_2O_6$; 3-$Al_2(SiO_4)(OH)_2$; 4-SiO_2; 5-Al_2SiO_5; 6-$ZnCO_3$; 7-$Ca_2Al(AlSiO_7)$; 8- $Zn_4Si_2O_7(OH)_2(H_2O)$; 9- $Al_4(OH)_8(Si_4O_{10})$; 10-$Na_4Cl(Al_3Si_3O_{12})$; 11-$Ca_{1.95}Al_{3.9}Si_{8.1}O_{24}(H_2O)$.

in Fig. 4. The dispersion hump peak at around 30° was observed in all tested specimens; it was generally related to the gel phase, such as N-A-S-H and C-(A)-S-H, which might be generated in the geopolymer composite by the reaction of the active ingredient MK and the alkali activator [35, 45]. Comparing the geopolymer specimens at 7 days and 28 days curing time, there was a reduction in the intensity of crystalline phases after long-time curing, indicating more transformation into amorphous and poorly crystalline gel phases with the extended curing time. Nevertheless, the formation of new amorphous compounds (gel) was difficult to identify owing to their coexistence and overlapping [45, 56]. Comparing the XRD patterns of BK0-28d, BK3-28d, and BK9-28d, the peak of $Al_4(OH)_8(Si_4O_{10})$ (kaolinite) was found only in BK0, but some new peaks overlapping with $ZnCO_3$ and $Zn_4Si_2O_7(OH)_2(H_2O)$ (hemimorphite) were noticed in BK3 and BK9. Specifically, $Al_4(OH)_8(Si_4O_{10})$ was derived from the raw materials that did not completely react. Zn mainly originated from the phytoremediation biowaste; the appearance of new phases of Zn indicated that the structure of the raw materials might be recombined, having undergone alkaline activation and polymerization. Noticeably, the peaks of $Na_4Cl(Al_3Si_3O_{12})$ and $Ca_{1.95}Al_{3.9}Si_{8.1}O_{24}(H_2O)$ decreased or disappeared in BK9-28d compared with BK9-7d, which might demonstrate the gradual decrease of zeolite-like N(C)-A-S-H. However, the peaks of $ZnCO_3$ and $Zn_4Si_2O_7(OH)_2(H_2O)$ appeared, and the structure of $Zn_4Si_2O_7(OH)_2(H_2O)$ was similar to that of N(C)-A-S-H. It can be inferred that Na(I) or Ca(II) in some N(C)-A-S-H phases might be replaced by Zn(II) and solidified/stabilized in the geopolymer structure, which was in agreement with the previous investigation [34, 50, 55]. Additionally, $Ca_2Al_3(Si_3O_{12})OH$ was observed in the geopolymer cured for 28 days, but was absent in BK9-7d. The polymer-like chain structure of $Ca_2Al_3(Si_3O_{12})OH$ could form stable chemical bonds with tetrahedrons [SiO_4] and [AlO_4] through dehydration reactions, which can promote the mechanical properties of the geopolymer composite [25, 57]. Prolonging the curing time is favorable for composite polymerization, as well as the solidification/stabilization of PTMs in the geopolymer composite.

FT-IR Analysis

The FT-IR spectra of BK0-28d, BK3-28d, BK9-28d, and BK9-7d specimens are shown in Fig. 5 to investigate the effect of biomass introduction and curing time on the molecular vibration modes and chemical groups of the geopolymer. The characteristic peak at around 3400 cm^{-1} represents the stretching vibration of O-H bonds, and 1640 cm^{-1} represents the bending vibration of O-H bonds, which indicates that water molecules were adsorbed on the surface or trapped in the pores of the geopolymer during the reaction [23, 26]. The peak of the O-H bond shifted from 3470.7 cm^{-1} (BK0-28d, absence of biomass) to 3439.4 cm^{-1} (BK3-28d, BK9-28d, and BK9-7d), suggesting the incorporation of biomass would affect the water absorption of geopolymers. More and more free water might transform into crystal water in [SiO_4] tetrahedron during the polymerization [18,

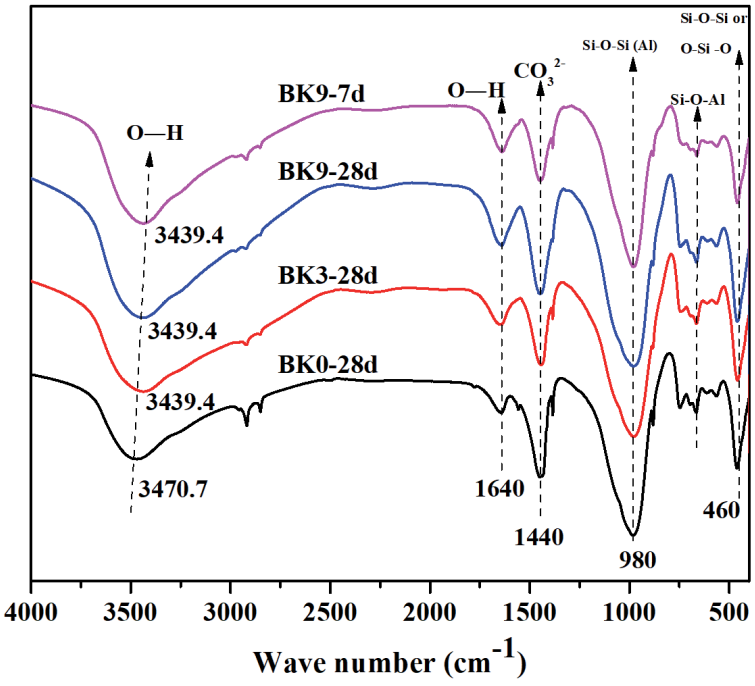

Fig. 5. FT-IR spectra of biomass-geopolymer.
Note: BK0-28d, BK3-28d, and BK9-28d represent the biomass-geopolymer curing for 28 days with biomass additions of 0 wt.%, 3 wt.%, and 9 wt.%, respectively; BK9-7d represents the biomass-geopolymer curing for 7 days with biomass addition of 9 wt.%.

35]. Absorption peaks appearing around ~1440 cm^{-1} were attributed to the symmetric stretching vibration of C-O bonds in the carbonate, which is partially from the introduction of raw materials or from the atmospheric geopolymer carbonation [44, 58]. The strongest absorption peaks of the specimens occurred at ~980 cm^{-1}, corresponding to the asymmetric stretching vibration of Si-O bonds in the middle-of-chain silicates of aluminosilicate chains [59]. It is characterized as the main structure of geopolymers and is generally applied for the identification of C-S-H gel phases [18]. Additionally, the absorption peak of Si-O bonds occurred at 981.1 cm^{-1} in BK0-28d, without biomass, slightly migrated to 980.6 $cm^{-1,}$ referring to BK3-28d, BK9-28d, and BK9-7d. Previous researchers [23, 27, 32, 50] suggested that this similar shift was caused by the formation of complex cation exchange layers around the Al-O bonds by heavy metal ions in the geopolymer, which could change the diffraction peaks of Si-O-Si or Si-O-Al. The bond energies of the four (Si-O or Al-O) bonds included in the [SiO_4] and [AlO_4] tetrahedron structure were uniform in the geopolymers. The trivalent Al in the oxide of Si or Al combines with four oxygen atoms, resulting in a negative charge for the [AlO_4] tetrahedron; thus, heavy metal ions could directly participate in the reaction to balance the charge in the system. Thus, Na (I) or Ca (II) sites are partially replaced, and PTMs were finally stabilized in the geopolymer system [60]. The ~690 cm^{-1} characteristic peak in the sample represents the bending vibration of Si-O-Al. Peaks around 460 cm^{-1} were the characteristic infrared peak of the bending vibration of O-Si-O bonds or the stretching vibration of Si-O-Si bonds [58]. It became stronger with the extended curing time, indicating a higher degree of silicate polymerization.

Practical Implications of this Study

The current research recommended that PTMs originating from phytoremediation biowaste could be effectively solidified/stabilized by the geopolymer composite, which can also be used as an insulation material due to the biomass addition. The special three-dimensional network structure could encapsulate the PTMs effectively, and the strong ion exchange capacity of the geopolymer might promote PTMs solidification. Due to its excellent mechanical and thermal insulation properties, particularly the superior performance in PTMs solidification/stabilization, the biomass-geopolymer composite is a promising green, energy-saving, and environmentally friendly material for the disposal of phytoremediation biowaste.

However, there are still some challenges in the present study. The active constituent of metakaolin could be partially replaced by some solid waste with similar components (such as fly ash, furnace slag, or rice husk ash) in order to achieve the elimination of waste. Many other potentially toxic metals (except zinc) are also included in the phytoremediation biowaste; it is difficult to identify their leaching performance or microstructure in the geopolymers owing to their low concentrations. Thus, more comprehensive and further investigation is needed to display the leachability and immobilization mechanism of various PTMs for the effective disposal of waste. In addition, a management system of environmental risk assessment and policy requirements is expected in future investigations.

Indeed, geopolymers can efficiently immobilize heavy metals through zeolite-like structures and porous characteristics, utilizing both chemical bonding and physical adsorption. This property makes geopolymers an ideal material for treating industrial wastewater, soil pollution, and tailings storage pollution, enabling them to replace traditional cement solidification techniques and reduce the risk of secondary pollution. Geopolymer-solidified composites can serve as substitutes for cement in the production of construction materials such as concrete and bricks. Their production consumes only 20%-30% of the energy required for ordinary Portland cement and reduces CO_2 emissions by 70%-80%, aligning with the requirements of the "dual carbon" goals (carbon peak and carbon neutrality). Additionally, geopolymers can be composited with reinforcing materials such as fibers and particles to produce high-strength, corrosion-resistant green building materials and high-performance composites for infrastructure repair. The pore structure of geopolymers can be adjusted and modified to fabricate efficient catalysts or heavy-metal adsorbents for applications in wastewater treatment, air purification, and other fields. Geopolymer technology can be integrated with other solid waste treatment techniques (such as incineration and landfilling) to form a closed-loop system that achieves "resource recovery, harmlessness, and reduction".

Conclusions

The preparation of geopolymer composite insulation material based on phytoremediation biowaste simultaneously achieved the goals of waste recovery, toxic metals immobilization, and high-performance material application. All specimens derived in this study presented superior compressive strength, and the compressive strength reached a maximum of 32.6 MPa when 3 wt.% biomass was added. For the specimen with 9 wt.% biomass addition, the thermal conductivity was 0.076 W/(m·K), which meets the requirement in the standard of Dry-mixed thermal insulating composition for buildings. Considering both the compressive strength and the thermal conductivity, 3 wt.% biomass addition is recommended for the biomass-geopolymer composite as insulation material for buildings, at which the highest compressive strength and considerable thermal conductivity are achieved. TCLP and SPLP leaching tests demonstrated that the S/S efficiency of Zn in all geopolymer specimens exceeded 98%, confirming the excellent PTMs solidification performance

of the geopolymer. Moreover, prolonging the curing time could significantly reduce the leachability of Zn. Microstructural characterization results indicated the existence of $ZnCO_3$ and $Zn_4Si_2O_7(OH)_2(H_2O)$, thereby revealing the solidification mechanism of Zn in the composite. The identification of the C–S–H gel phase proved the main representative structure in the geopolymer specimens, which played an important role in PTMs solidification/stabilization. In summary, the method of using phytoremediation biowaste to prepare geopolymers has the potential for immobilizing toxic metals, treating solid waste, and producing insulation composite materials.

Acknowledgments

This work was supported by the Youth Fund for Scientific Research and Development of Rocket Force University of Engineering under Grant 2022QN-B008.

Conflict of Interest

The authors declare no conflict of interest.

References

1. DU J., ZHANG L., ALI A., LI R., XIAO R., GUO D., LIU X., ZHANG Z., REN C., ZHANG Z. Research on thermal disposal of phytoremediation biowaste: Stability of potentially toxic metals (PTMs) and oxidation resistance of biochars. Process Safety and Environment Protection. **125**, 260, **2019**.
2. KOVACS H., SZEMMELVEISZ K. Disposal options for polluted plants grown on heavy metal contaminated brownfield lands – a review. Chemosphere. **166**, 8, **2017**.
3. XIAO R., SHEN F., DU J., LI R., LAHORI A.H., ZHANG Z. Screening of native plants from wasteland surrounding a Zn smelter in Feng County China, for phytoremediation. Ecotoxicology and Environment Safety. **162**, 178, **2018**.
4. XU Z.Y., MUCHANGOS L.S., ITO L., TOKAI A. Cost and health benefit analysis of remediation alternatives for the heavy-metal-contaminated agricultural land in a Pb–Zn mining town in China. Journal Of Cleaner Production. **397**, **2023**.
5. DASTYAR W., RAHEEM A., HE J., ZHAO M. Biofuel production using thermochemical conversion of heavy metal-contaminated biomass (HMCB) harvested from phytoextraction process. Chemical Engineering Journal. **358**, 759, **2019**.
6. WANG S., GAO B., LI Y., OK Y.S., SHEN C., XUE S. Biochar provides a safe and value-added solution for hyperaccumulating plant disposal: a case study of Phytolacca acinosa Roxb. (*Phytolaccaceae*). Chemosphere. **178**, 59, **2017**.
7. SINGH J., KALAMDHAD A.S. Concentration and speciation of heavy metals during water hyacinth composting. Bioresource Technology. **124**, 169, **2012**.
8. BARBAROUX R., MEUNIER N., MERCIER G., TAILLARD V., MORE J.L., SIMONNOT M.O., BLAIS J.F. Chemical leaching of nickel from the seeds of the metal hyperaccumulator plant Alyssum murale. Hydrometallurgy. **100** (1-2), 10, **2009**.
9. NUNEZ-LOPEZ R.A., MEAS Y., GAMA S.C., BORGES R.O., OLGUIN E.J. Leaching of lead by ammonium salts and EDTA from Salvinia minima biomass produced during aquatic phytoremediation. Journal of Hazardous Materials. **154** (1-3), 623, **2008**.
10. ZHONG D.X., ZHONG Z.P., WU L.H., DING K., LUO Y.M., CHRISTIE P. Pyrolysis of Sedum plumbizincicola, a zinc and cadmium hyperaccumulator: pyrolysis kinetics, heavy metal behaviour and bio-oil production. Clean Technologies and Environmental Policy. **18**, 2315, **2016**.
11. JIANG H.W., CHEN X.F., CHEN S.K., LI H.G., PENG Y., ZHU A.G., XU C.B.C., YANG W.R. Recovery of arsenic and practical utilization of aqueous phase in hydrothermal liquefaction of hyperaccumulator Chemical Engineering Journal. **439**, 135514, **2022**.
12. SUI H.Q., JIANG H., LI G., CHEN J.F., CHENG W., CHEN H.P. Combustion of phytoremediation biomass for recycling utilization: Thermal behavior, kinetic analysis, and release of heavy metal. Industrial Crops & Products. **230**, 121047, **2025**.
13. DU J., ZHANG L., LIU T., XIAO R., LI R., GUO D., QIU L., YANG X., ZHANG Z. Thermal conversion of a promising phytoremediation plant (Symphytum officinale L.) into biochar: Dynamic of potentially toxic elements and environmental acceptability assessment of the biochar. Bioresource Technology. **274**, 73. **2019**.
14. HUANG H., YAO W., LI R., ALI A., DU J., GUO D., XIAO R., GUO Z., ZHANG Z., AWASTHI M.K. Effect of pyrolysis temperature on chemical form, behavior and environmental risk of Zn, Pb and Cd in biochar produced from phytoremediation residue. Bioresource Technology. **249**, 487, **2018**.
15. LI S., CHEN G. Thermogravimetric, thermochemical, and infrared spectral characterization of feedstocks and biochar derived at different pyrolysis temperatures. Waste Management. **78**, 198, **2018**.
16. O'CONNOR D., PENG T., ZHANG J., TSANG D.C.W., ALESSI D.S., SHEN Z., BOLAN N.S., HOU D. Biochar application for the remediation of heavy metal polluted land: a review of in situ field trials. Science of the Total Environment. **619-620**, 815, **2018**.
17. LI Z.Y., HUANG Y.J., ZHU Z.C., YU M.Z., CHENG H.Q., SHI H., XIAO Y.X., SONG H.K., ZUO W., ZHOU H.Y., WANG S. Attempts to obtain clean biochar from hyperaccumulator through pyrolysis: Removal of heavy metals and transformation of phosphorus. Journal of Hazardous Materials. **468**, 133837, **2024**.
18. FAN C., WANG B., AI H., QI Y., LIU Z. A comparative study on solidification/stabilization characteristics of coal fly ash-based geopolymer and Portland cement on heavy metals in MSWI fly ash. Journal Of Cleaner Production. **319**, **2021**.
19. RASAKI S.A., ZHANG B.X., GUARECUCO R., THOMAS T., YANG M.H. Geopolymer for use in heavy metals adsorption, and advanced oxidative processes: a critical review. Journal Of Cleaner Production. **213**, 42, **2019**.
20. WANG S.Y., LIU B., ZHANG Q., WEN Q., LU X.H., XIAO K., EKBERG C., ZHANG S.G. Application of geopolymers of treatment of industrial solid waste containing heavy metals: State of the art review. Journal Of Cleaner Production. **390**, **2023**.

21. PU S.Y., SHEN Z.W., DUAN W., LANG L., LIU Y., XU B.M., YAO H.R., MEI G.X. Discussion on the applicability and mechanism of phosphate-based geopolymers used for cadmium and cadmium-lead heavy metals solidification/stabilization. Journal Of Environmental Chemical Engineering. **12**, **2024**.
22. DAVIDOVITS J. Geopolymers – inorganic polymeric new materials. Journal Of Thermal Analysis and Calorimetry. **37**, 1633, **1991**.
23. XIA M., MUHAMMAD F., ZENG L., LI S., HUANG X., JIAO B., SHIAU Y., LI D. Solidification/stabilization of lead-zinc smelting slag in composite based geopolymer. Journal Of Cleaner Production. **209**, 1206, **2019**.
24. ZOU S., LI H., WANG S., JIANG R., ZOU J., ZHANG X., LIU L., ZHANG G. Experimental research on an innovative sawdust biomass-based insulation material for buildings. Journal Of Cleaner Production. **260**, **2020**.
25. LIU J.R., DOH J.H., ONG DOMINIC E.L., DINH H.L., PODOLSKY Z., ZI G. Investigation on red mud and fly ash-based geopolymer: Quantification of reactive aluminosilicate and derivation of effective Si/Al molar ratio. Journal of Building Engineering. **71**, **2023**.
26. CHEN C.L., LIU H., ZHANG Y., GU G.H., HU J.Y. Micro-assessment of heavy metal immobilization within alkali-activated copper tailings-slag geopolymer. Cement and Concrete Composites. **149**, 105510, **2024**.
27. SUN M.Y., MA L.P., DAI Q.X., YANG J., XIE L.G., HU Y., DUAN L., YAN X., ZHOU G.Y., ZENG L.L., SHAO L., HU B., YAN Q.C. Preparation of functional geopolymers from municipal solid waste incineration fly ash: An approach combining experimental and computational simulation studies. Journal of Environmental Management. **355**, **2024**.
28. LU X., GUO J.F., CHEN F., TIAN M.K. Synthesis of ternary geopolymers using prediction for effective solidification of mercury in tailings. Journal of Environmental Sciences. **147**, 392, **2025**.
29. REN B., ZHAO Y.L., BAI H.Y., KANG S.C., ZHANG T.T., SONG S.X. Eco-friendly geopolymer prepared from solid wastes: A critical review. Chemosphere, **267**, 128900, 2021.
30. FREIRE A.L., SILVA A D.A., ROCC D.G.D., SALLA J D.A.S., PERGHER S.B.C, RODRÍGUEZ-CASTELLÓN E., JOSÉ H.J., MOREIRA R DA F.P.M. Synthesis and characterization of geopolymers based on phosphate mining tailings and its application for carbon dioxide and nitrogen adsorption. Ceramics International. **51**, 8396, **2025**.
31. SU L.J., LI S.Q., WU S.Y., LIANG B., ZHANG X.D. Preparation and heavy metal solidification mechanism of physically activated municipal solid waste incineration fly ash base geopolymer backfill. Process Safety and Environmental Protection. **201**, 107522, **2025**.
32. JI Z.H., SU L.Y., PEI Y.S. Synthesis and toxic metals (Cd, Pb, and Zn) immobilization properties of drinking water treatment residuals and metakaolin-based geopolymers. Materials Chemistry and Physics. **242**, **2020**.
33. CHEN Y.C., CHEN F.Y., ZHOU F., LU M., HOU H.B., LI J.P., LIU D.M., WANG T. Early solidification/stabilization mechanism of heavy metals (Pb, Cr and Zn) in Shell coal gasification fly ash based geopolymer. Science of the Total Environment. **820**, **2022**.
34. ZHANG Y., LIU H., MA T., CHEN C.L., GU G.H., WANG J.H., SHANG X. Experimental assessment of utilizing copper tailings as alkali-activated materials and fine aggregates to prepare geopolymer composite. Construction and Building Materials. **408**, **2023**.
35. HAN Y.J., QI W.Y., PANG H.T., ZHAO Q.X., HUANG Y.L., ZHAO D.Z., ZHU W.H., ZHANG J.H. A novel coal gasification coarse slag-based geopolymer: Influences of physico-chemical coupling activation on its properties, microstructure, and hazardous material immobilization. Construction and Building Materials. **420**, **2024**.
36. DU J., GUO Z., LI R., ALI A., GUO D., LAHORI A.H., WANG P., LIU X., WANG X., ZHANG Z. Screening of Chinese mustard (*Brassica juncea* L.) cultivars for the phytoremediation of Cd and Zn based on the plant physiological mechanisms. Environmental Pollution. **261**, **2020**.
37. WANG Y., HAN F., MU J. Solidification/stabilization mechanism of Pb(II), Cd(II), Mn(II) and Cr(III) in fly ash based geopolymers. Construction and Building Materials. **160**, **2018**.
38. ZHANG H., JI Z., ZENG Y., PEI Y. Solidification/stabilization of landfill leachate concentrate contaminants using solid alkali-activated geopolymers with a high liquid solid ratio and fixing rate. Chemosphere. **288**, **2022**.
39. ZHANG Q., CAO X., SUN S., YANG W., FANG L., MA R., LIN C., LI H. Lead zinc slag-based geopolymer: Demonstration of heavy metal solidification mechanism from the new perspectives of electronegativity and ion potential. Environmental Pollution. **293**, **2022**.
40. Thermal insulation-Determination of steady-state thermal resistance and related properties-Guarded hot plat apparatus (ISO8302: 1991, IDT; GB/T10294-2008, China). **1991**.
41. US Environmental Protection Agency. Method 1311: Toxicity Characteristic Leaching Procedure. Washington, DC, **1992**.
42. US Environmental Protection Agency. Method 1312: Synthetic precipitation leaching procedure. Washington, DC, **1992**.
43. PRC Ministry of Ecology and Environment. Identification Standards for Hazardous Wastes-Identification for Extraction Toxicity (GB5085.3-2007), Beijing, China, **2007**.
44. BAH A., JIN J., RAMOS A.O., BAO Y., MA M., LI F. Arsenic(V) immobilization in fly ash and mine tailing-based geopolymers: Performance and mechanism insight. Chemosphere. **306**, **2022**.
45. ZHAO S., XIA M., YU L., HUANG X., JIAO B., LI D. Optimization for the preparation of composite geopolymer using response surface methodology and its application in lead-zinc tailings solidification. Construction and Building Materials. **266**, **2021**.
46. US Environmental Protection Agency. Method 3051A: Microwave Assisted Acid Digestion of Soils. Washington, DC, **1992**.
47. ZHENG Y.H., WANG Z., WAN Z.M., YANG X., LIN F.C., CHEN Y.D., TANG L.R., LIN G.F., LU Q.L., HANG B., LU B.L. Mechanochemical fabrication of geopolymer composites based on the reinforcement effect of microfibrillated cellulose. Ceramics International. **49**, 503, **2023**.
48. YE H., ZHANG Y., YU Z., MU J. Effects of cellulose, hemicellulose, and lignin on the morphology and mechanical properties of metakaolin-based geopolymer. Construction and Building Materials. **173**, 10, **2018**.
49. LIU L., ZOU S., LI H., DENG L., BAI C., ZHANG X., WANG S., LI N. Experimental physical properties of an

eco-friendly bio-insulation material based on wheat straw for buildings. Energy and Buildings. **201**, 19, **2019**.
50. WANG S. Experimental study on preparation of building insulation materials by rice husk and geopolymer composite. Dissertation, Hunan University, China, **2018**. [in Chinese]
51. CN-GB. Dry-mixed thermal insulating composition for buildings (GB/T 20473-2006), Beijing, China, **2006**.
52. WANG S., LI H., ZOU, S., LIU L., BAI C., ZHANG G., FANG L. Experimental study on durability and acoustic absorption performance of biomass geopolymer-based insulation materials. Construction and Building Materials. **361**, **2022**.
53. CHIU A.C.F., AKESSEH R., MOUMOUNI I.M., XIAO Y. Laboratory assessment of rice husk ash (RHA) in the solidification/stabilization of heavy metal contaminated slurry. Journal of Hazardous Materials. **371**, 62, **2019**.
54. AN S., WANG B.M., CHEN W.X., YU Z., FAN C.C. Preparation of geopolymer based on municipal solid waste incineration fly ash-phosphorus slag and its function for solidification of heavy metals. Waste Manage. **178**, 186, **2024**.
55. EL-ESWED B.I., ALDAGAG O.M., KHALILI F.I. Efficiency and mechanism of stabilization/solidification of Pb(II), Cd(II), Cu(II), Th(IV) and U(VI) in metakaolin based geopolymers. Applied Clay Science. **140**, 148, **2017**.
56. CAO L.Q., ZUO Y.B., LIANG S., SUN Y.F., KE Y., YANG J.K., WEI X.S., HU J.P., HOU H.J. Geopolymerization of MSWI fly ash and coal fly ash for efficient solidification of heavy metals: Insights into stabilization mechanisms and long-term leaching behavior. Construction and Building Materials. **411**, **2024**.
57. WAN Q., RAO F., SONG S., ZHANG Y. Immobilization forms of ZnO in the solidification/stabilization (S/S) of a zinc mine tailing through geopolymerization. Journal of Materials Research and Technology. **8** (6), 5728, **2019**.
58. KARTHIK A., SUDALAIMANI K., VIJAYAKUMAR C.T., SARAVANAKUMAR S.S. Effect of bio-additives on physico-chemical properties of fly ash-ground granulated blast furnace slag based self-cured geopolymer mortars. Journal of Hazardous Materials. **361**, 56, **2019**.
59. LONG W.J., LIN C., YE T.H., DONG B., XING F. Stabilization/solidification of hazardous lead glass by geopolymers. Construction and Building Materials. **294**, **2021**.
60. ZAWRAH M.F., GADO R.A., FELTIN N., DUCOURTIEUX S., DEVOILLE L. Recycling and utilization assessment of waste fired clay bricks (Grog) with granulated blast-furnace slag for geopolymer production. Process Safety and Environmental Protection. **103**, 237, **2016**.